Systematic Characterization Framework of Row-Column Ultrasound Imaging Systems

by

Ibrahim Ben Daya

A thesis
presented to the University of Waterloo
in fulfillment of the
thesis requirement for the degree of
Master of Science
in
System Design Engineering

Waterloo, Ontario, Canada, 2015

I hereby declare that I am the sole author of this thesis. This is a true copy of the thesis, including any required final revisions, as accepted by my examiners.

I understand that my thesis may be made electronically available to the public.

Abstract

3-D ultrasound imaging offers unique opportunities in the field of non-destructive testing that cannot be easily found in A-mode and B-mode images. To acquire a 3-D ultrasound image without a mechanically moving transducer, a 2-D array can be used. The row column technique is preferred over a fully addressed 2-D array as it requires a significantly lower number of interconnections. Recent advances in 3-D row-column ultrasound imaging systems were largely focused on sensor design. However, these imaging systems face three intrinsic challenges which cannot be addressed by improving sensor design alone: speckle noise, sparsity of data in the imaged volume, and the spatially dependant point spread function of the imaging system. There is no characterization model that describes these intrinsic challenges.

In this research, we will propose a characterization framework for ultrasound imaging systems that are based on the row column method. The proposed framework will include a joint statistical image formation and noise modeling and characterization as well as a characterization of the system's beam profile using a spatially-variant point spread function.

Our proposed framework has many potential applications including building a more adequate image reconstruction model, providing a better metric for comparison of different row column systems, allowing for a better optimization of a row column system's performance, and giving us a better understanding of images acquired from row column systems.

Acknowledgements

For his continuous motivation, guidance and support during my time in the VIP lab, I would like to thank Prof. Alexander Wong. No matter how busy you were, you always made time for me. Thank you for being patient. I couldn't have written this without you, and I look forward working with you again.

For helping me better understand ultrasound in general and row column in particular, I would like to thank Prof. John Yeow and Albert Chen. My research was made easier with your guidance.

I would like to thank Prof. David Clausi and Prof. Andrea Scott, for taking the time out of their busy schedule to read and review my thesis.

To Mom and Dad: thanks for supporting me all these years. The food was good. The company better.

To my big brother: thank you for all the times you let me beat you at FIFA. It was always a good distraction.

To Melik and Yue: thanks for all the coffee.

Dedication

In loving memory of Mustapha (1992 - 2006) and Elina (1989 - 2011). My inner child died with you, I hope he's a better company than I was.

Table of Contents

List of Tables

List of Figures

Chapter 1

Introduction

1.1 Motivation

This section will detail the motivation behind this thesis. First we will show the value of three dimensional ultrasound imaging in different applications, and then we will discuss why the row-column method is ideal for three dimensional ultrasound imaging.

1.1.1 Three Dimensional Ultrasound

Ultrasound imaging is a valuable tool in non-destructive testing (NDT), with applications ranging from detection of material defects to object and foreign body detection. Three dimensional ultrasound imaging offers the possibility of accurately generating certain material properties that could be useful to material scientists [27]. Three dimensional ultrasound imaging could also be useful in medical imaging: to image the same slice in two dimensions for the purpose of follow up studies is difficult, and viewing of anatomy using a two dimensional imaging device requires a great deal of skill and experience [29].

When designing three dimensional ultrasound imaging systems, electronic beam-steering with a fixed transducer is preferred over a mechanically moving one, as mechanical motion introduces unwanted artifacts and increases image acquisition time [22]. A mechanically fixed two dimensional array of transducers is capable of acquiring a three dimensional ultrasound image [29]. However, in a fully addressed two dimensional array, the total number of elements scales with the square of the number of elements in each dimension [22]. This leads to an impractical number of interconnections (since every individual element needs to

be addressed) and significant amount of data to handle, posing a challenge both in terms of real time data processing and the actual fabrication of connections.

1.1.2 Row-Column Method

In this method, a pair of orthogonally positioned one dimensional arrays of rows and columns, where one is responsible for transmit beamforming and the other for receive beamforming, is used. Just like the fully addressed two dimensional array, this method does not require mechanical motion. However, the number of connection is significantly less when compared to the fully addressed array.

Since row-column only focuses in azimuth for transmit and elevation for receive, beamforming relies on natural focusing for elevation during transmit and azimuth during receive [29]. Therefore, the focusing power for row-column beamforming scheme is limited. Pressure near the transducer significantly varies as sound emitted from different parts of the transducer interferes constructively and destructively. The variation in pressure decreases as sound travels away from the transducer, creating a varying beam profile that changes the response of the imaging system with depth. This varying beam profile poses a challenge when it comes to image reconstruction, as it will require incorporating a spatially dependant point spread function into the reconstruction framework.

Three dimensional reconstruction of ultrasound images poses some other interesting challenges. Real-time three dimensional imaging requires finite transmit events, meaning that the readings of the scanner are inherently sparse; what needs to be done is recover the full three dimensional image of the target object from incomplete data. Another challenge is the nature of speckle noise that is inherent to ultrasound images, and how it should be modeled. While the issue of sparsity and noise have been addressed in the literature [10, 18], the problem with spatially dependant point spread function for row-column ultrasound imaging has not been fully explored.

Having a characterization framework for these challenges (data sparsity, speckle noise, and spatially dependant point spread function) can be very helpful for the row-column method. This framework can provide a strong basis for a powerful compensated reconstruction model for three dimensional ultrasound imaging systems that use the row-column method, give us a more accurate metric for comparison of different row-column ultrasound imaging systems, allow of better optimization of row-column ultrasound imaging systems, and give us a better understanding of the images we get from row-column ultrasound imaging systems.

1.2 Thesis Contributions

The ultimate goal of this thesis is to provide a mathematical characterization framework specifically for row-column imaging systems. By understanding how an image from a row-column system is formed, studying the speckle noise, and studying the varying beam profile of row-column systems, we hope to create a strong characterization framework to be later used as the basis of a three dimensional row-column image reconstruction model as well as to be used to build an evaluation method for the comparison of different systems. Such a framework would also help with the optimization of the imaging system's performance, and would help us better understand the images produced. The thesis contributions are:

- We will formulate a mathematical expression of how an image is formed in a row-column system. This will help with the understanding of the sparsity of data in a three dimensional ultrasound image.
- We will find the optimal noise model for ultrasound speckle noise from data acquired with row-column systems.
- We will formulate a mathematical expression of the row-column's varying beam profile and use it as a basis for estimating the point spread function (PSF) of the row-column system.

1.3 Thesis Outline

- Chapter 2: discusses background information on ultrasound imaging with a focus on the row-column system. It will contain a brief history of ultrasound, a mathematical formulation of the physical properties of ultrasound, and a brief overview of the row-column sysstem.
- Chapter 3: provides mathematical formulation of how an image is formed as well as a mathematical formulation of speckle noise in ultrasound
- Chapter 4: discusses characterization of row-column beam profile
- Chapter 5: concludes this thesis by providing a summary of what was discussed and give suggestions for future work

Chapter 2

Background

This chapter provides fundamental information on the row-column imaging system. First we give a brief overview of the history of ultrasound, next we discuss the main physical properties of ultrasound: acoustic wave propagation and wave attenuation. Finally, we discuss the generation and reception of ultrasound waves from one dimensional arrays to the full row-column addressing scheme, which will be the focus of this thesis.

2.1 History of Ultrasound

The science of sound dates as far back as the 6th century BC when Pythagoras wrote mathematical properties of stringed instruments. The use of sound as a diagnostic tool was first foreseen by English scientist Robert Hooke (most notably know for the theory of elasticity) when he wrote [29]:

> "It may be possible to discover the motions of the internal parts of bodies, whether animal, vegetable, or mineral, by the sound they make; that one may discover the works performed in the several offices and shops of a man's body, and thereby (sic) discover what instrument or engine is out of order, what works are going on at several times, and lie still at others, and the like. I could proceed further, but methinks I can hardly forbear to blush when I consider how the most part of men will look upon this: but, yet again, I have this encouragement, not to think all these things utterly impossible"

However, the first attempt at a technological application of ultrasound was inspired by the Titanic tragedy. In 1913, one month after the Titanic hit the iceberg, British scientist L. F. Richardson filed patents to use underwater echo-ranging to detect icebergs. Ultrasound imaging has since evolved to be used in applications ranging from detection of material defects and foreign body detection in non destructive testing to medical diagnostics.

All ultrasound imaging systems follow the same basic principle: a sound pulse is generated by a transducer, this sound pulse is transmitted into a medium which contains an object of interest, at those different boundaries echoes will be reflected, and these reflected echos will be received by a transducer to form an ultrasound image.

2.2 Physical Properties of Ultrasound

2.2.1 Acoustic Wave Propagation

Just like all sound waves, an ultrasound wave propagates in a similar manner to a wave of mechanical vibrations. Pressure disturbances created from the ultrasound source cause local oscillatory movements from one group of atoms to the next along the direction of the wave's travel. Although wave propagation for ultrasound falls under one of three types: plane, spherical, or cylindrical (shown in Figure 2.1), the shape of the wave will generally change in more complicated ways. However, to be able to characterize ultrasound systems, we must write down mathematical equations for such propagations.

Wave Equations for Fluids and Solids

Fluid waves are longitudinal in nature: one that travels along its propagation direction while making the particles move back and forth in a sinusoidal motion. If we can define u as the displacement of particles from their equilibrium state at particle velocity v as the wave passes through the medium, and if we define p as the local pressure disturbances resulting from the passage of such waves, we can come up with a set of equations that characterize wave motion in fluids.

In an ideal fluid, one that has no or negligible viscosity, particle velocity v can be expressed in terms of displacement as:

$$v = \frac{\partial u}{\partial t} \tag{2.1}$$

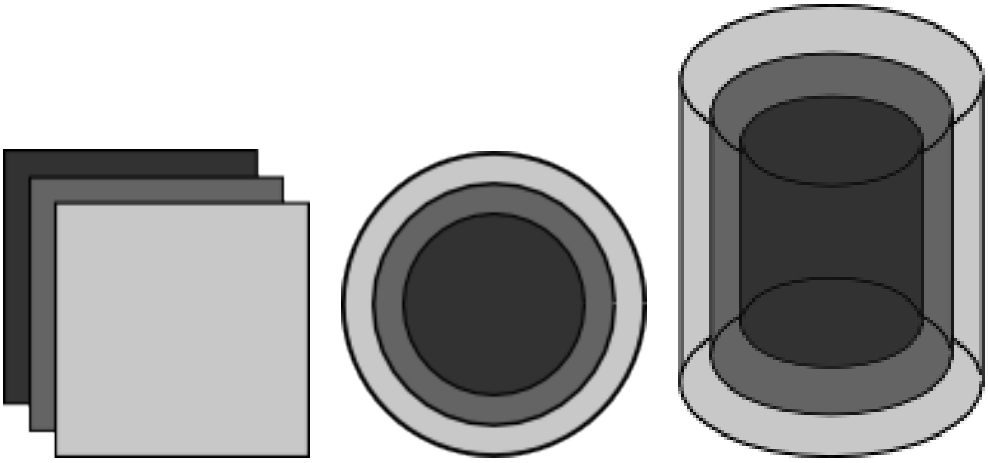

(a) Plane Wave (b) Spherical Wave (c) Cylindrical Wave

Figure 2.1: Possible types of ultrasound wave propagation [29]

For convenience, we define a velocity potential ϕ, and equation 2.1 can be rewritten as:

$$v = \nabla\phi \tag{2.2}$$

Pressure can then be defined as:

$$p = -\rho\frac{\partial\phi}{\partial t} \tag{2.3}$$

where ρ is the density of the fluid at rest. If we set the direction of the wave along the z axis, the equation (in Cartesian coordinates) that governs one dimensional wave travel can be written as:

$$\frac{\partial^2\phi}{\partial z^2} - \frac{1}{c_L^2}\frac{\partial^2\phi}{\partial t^2} = 0 \tag{2.4}$$

where c_L is the longitudinal speed of sound, which is defined by the fluid's specific heat γ, density ρ_0, and isothermal bulk modulus B_T following the equation:

$$c_L = \sqrt{\frac{\gamma B_T}{\rho_0}} \tag{2.5}$$

One interesting property to take into account is the specific characteristic impedance (sometimes referred to as the specific acoustic impedance) often denoted by Z, and is defined as the ratio of a forward travelling pressure wave to the particle velocity of the fluid:

$$Z_L = \frac{p}{v_L} = \rho_0 c_L \tag{2.6}$$

The plane wave equation (2.4) can be generalized to three dimensions through introducing the notation ϕ_{tt} as:

$$\nabla^2 \phi - \frac{1}{c^2}\phi_{tt} = 0 \tag{2.7}$$

where ϕ_{tt} simply:

$$\phi_{tt} = \frac{\partial^2 \phi}{\partial t^2} \tag{2.8}$$

Following this, the spherical wave equation can be expressed as:

$$\phi_{rr} + \frac{2}{r}\phi_r - \frac{1}{c^2}\phi_{tt} = 0 \tag{2.9}$$

and the cylindrical wave equation can be expressed as:

$$\phi_{rr} + \frac{1}{r}\phi_r - \frac{1}{c^2}\phi_{tt} = 0 \tag{2.10}$$

where r is the radial distance.

The general solution to the plane wave equation (2.4) is given by:

$$\phi(z,t) = g(t - \frac{z}{c_L}) + h(t + \frac{z}{c_L}) \tag{2.11}$$

where g is the term representing waves that are traveling along the positive z axis, and h represents waves traveling along the negative z axis.

The general solution to the spherical wave equation (2.9) is given by:

$$\phi(z,t) = \frac{g(t - \frac{z}{c_L})}{r} + \frac{h(t + \frac{z}{c_L})}{r} \tag{2.12}$$

For the cylindrical wave equation (2.10) the only estimated solution is available is for large distances r, given by:

$$\phi(z,t) \approx \frac{g(t-\frac{z}{c_L})}{\sqrt{r}} + \frac{h(t+\frac{z}{c_L})}{\sqrt{r}} \tag{2.13}$$

Although fluids only support longitudinal waves, solids are capable of supporting shear waves as well as longitudinal ones. However, for the majority of applications that use ultrasound, longitudinal waves are of the main interest.

As far as mathematical formulation goes for longitudinal waves in solids, stress replaces pressure in the equations (2.1) through (2.4), and the basic relationships are the same.

One Dimensional Wave Reflection off Boundries

Since most objects have rough boundaries and not ideal plain ones, the pattern of reflected waves from most objects is very complex. Most of these waves do not return to the receiver, the detected "back-scatter" is simply a fraction of the total information present in the ultrasound field.

To formulate some kind of relationship between the transmitted and reflected component of the wave, we will consider an ideal medium with an acoustic impedance Z_1 that a plane wave is propagating through and it bounces of an ideal plain boundary of an acoustic impedance of Z_2. The pressure at the boundary can be formulated in a manner analogous to a voltage drop across Z_2:

$$p_2 = p_0(1+RF) \tag{2.14}$$

where p_0 is the pressure of the transmitted wave, and RF is the reflection coefficient: a factor that describes how much of the pressure wave is reflected by the impedance difference.

The particle velocity can be expressed in a similar way to the sum of currents flowing in a transmission line in the opposite direction:

$$v_2 = \frac{(1-RF)p_0}{Z_1} \tag{2.15}$$

The acoustic impedance (measured in Rayls) can be found using equation 2.6:

$$Z_2 = \frac{p_2}{v_2} = \frac{(1+RF)Z_1}{1-RF} \tag{2.16}$$

Rewriting equation 2.16, we can find an expression for RF:

$$RF = \frac{Z_2 - Z_1}{Z_2 + Z_1} \tag{2.17}$$

2.2.2 Attenuation

Ultrasound waves encounter losses as they propagate through real media. Pressure waves lose energy to the surrounding medium just as forces encounter friction, which often results in local heating. These losses are referred to as "attenuations" and are most commonly formulated using exponential expressions with distance. For an ultrasound wave with center frequency f_c, its amplitude as a function of distance and time can be expressed as:

$$A(z,t) = A_0 \exp\big(i(2\pi f_c t - kz)\big) \exp\big(-\alpha z\big) \tag{2.18}$$

where α is the attenuation coefficient, usually expressed in nepers per centimeter, and k is the wavenumber.

Time Gain Compensation

Imaging systems incorporate a method called Time Gain Compensation to account for the affects energy loss in media. By knowing the penetration depth of the imaging system beforehand, the depth dimension of the image can be divided into strips connected to separate amplifier stages. These amplifiers are adjusted to boost amplitude with depth in an effort to counteract the affects of attenuation.

2.3 Ultrasound Wave Generation and Reception

2.3.1 Transducers

The transducer is the part of the ultrasound imaging system responsible for the transmission and reception of ultrasound waves. Although the majority of commercially available

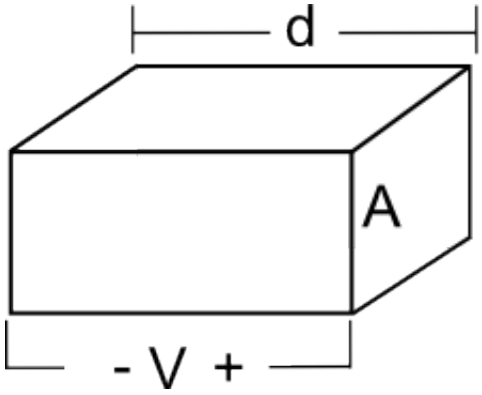

Figure 2.2: The simplest form of a piezoelectric transducer. V is the applied voltage impulse, d is the thickness of the transducer, A is the cross sectional area of the transducer. [29]

systems use piezoelectric transducers, an emerging generation of transducers called capacitive micromachined ultrasonic transducers (CMUTs) has shown great potential that could replace them. Both piezoelectric transducers and CMUTs will be discussed.

Piezoelectric transducers

Piezoelectric crystals are materials that exhibit a strain when placed under an electric potential. When a voltage pulse is applied across a piezoelectric crystal, a wave pressure will be released into the surrounding medium as a result of the crystal's contraction and expansion. This crystals will also output a voltage potential when it experiences strain from an incoming wave pressure, which can then be amplified and measured.

Figure 2.2 shows the simplest piezoelectric transducer. It consists of a piezoelectric crystal with electrodes at the top and bottom. The transducer has a thickness d and across section A, both of which govern the clamped capacitance according to the equation:

$$C_0 = \varepsilon^S \frac{A}{d} \tag{2.19}$$

where ε^S is the clamped dielectric constant.

When a voltage impulse V is applied across the transducer's electrodes, the force at the top and bottom of the transducer generated by the piezoelectric effect is given by:

$$F(t) = \left(\frac{\iota}{2} C_0 V\right)\left[- \delta(t) + \delta(t - \frac{d}{c})\right] \tag{2.20}$$

where ι is the piezoelectric constant.

The transducer's fundamental resonant frequency is dependant on the thickness:

$$f_0 = \frac{c}{2d} \tag{2.21}$$

where c is the speed of sound between the two electrodes, given by:

$$c = \sqrt{\frac{C^D}{\rho}} \tag{2.22}$$

where C^D is the elastic stiffness constant.

When operating at a frequency near to a piezoelectric material's resonant frequency, these materials are capable of generating an ultrasound wave with a relatively large amplitude power. Since the thickness of the piezo layer determines its resonance frequency(equation 2.21), a piezoelectric transducer must be chosen with care to work at the desired frequency, this limits the operation of that transducer at range close to that frequency.

One of the drawbacks of using piezoelectric materials as transducers is their high acoustic impedance when compared to that of the medium. Most transducers have an acoustic impedance of around 30 MRayl, while water and air have an acoustic impedance of 1.5 and 400 MRayl. Another drawback stems from the relationship between frequency and element pitch in phased arrays, where there is a tight tolerance when high frequency element arrays (both one and two dimensional) are fabricated. The necessary cuts that must to be made to each individual element (particularly in two dimensional ones) greatly reduce the active area of the element. These drawbacks were the some of the main motivations behind CMUTs.

Capacitive Micromachined Ultrasonic Transducers

The idea of generating and receiving sound through electrostatic means was first demonstrated by Edison Dolbear in the late 19th century. Electrostatic based ultrasound transducers, termed CMUTs, have generated great interest in the mid 1990s.

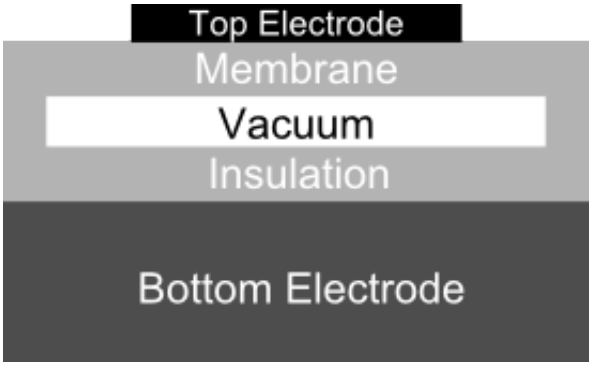

Figure 2.3: A schematic of the cross section of a simple CMUT cell.

The basic CMUT unit (often referred to as "cell") is shown in Figure 2.3. It consists of a thin membrane suspended over a shallow cavity, with a patterned electrode on its top and a fixed electrode at the bottom.

CMUT's actuation is quite similar to that of its piezoelectric counter part. When a voltage pulse is applied, the membrane vibrates as electrostatic forces begin to be released. Some of the energy escapes into the surrounding media as pressure waves. Conversely, when an incoming pressure wave hits the membrane and causes it to vibrate, the capacitance of the cell will change which induces a current. This can be understood through the relationship:

$$C = \frac{q}{V} \tag{2.23}$$

where C, q and V are the capacitance, charge and voltage respectively.

However, one difference between the actuation of CMUTs and piezoelectric transducers is that CMUTs need a DC bias across the capacitor, both at transmit and receive. Because of this DC bias, the potential is fixed.

The main advantage CMUTs have over piezoelectric transducers is the way they are fabricated. With currently available microfabrication techniques, it is possible to achieve sub-micron feature sizes. Defining accurate element layout and repeatedly manufacture arrays with those elements is made very easy. This is particularly ideal for high frequency two dimensional arrays as element size needs to be small (CMUTs piezoelectric counterpart relies on the conventional dice-and-fill, which makes reliable layout definitions of elements very challenging). Parallel processing techniques for semiconductor fabrication enable the production of thousands of devices simultaneously, which greatly reduces the cost of fabrication.

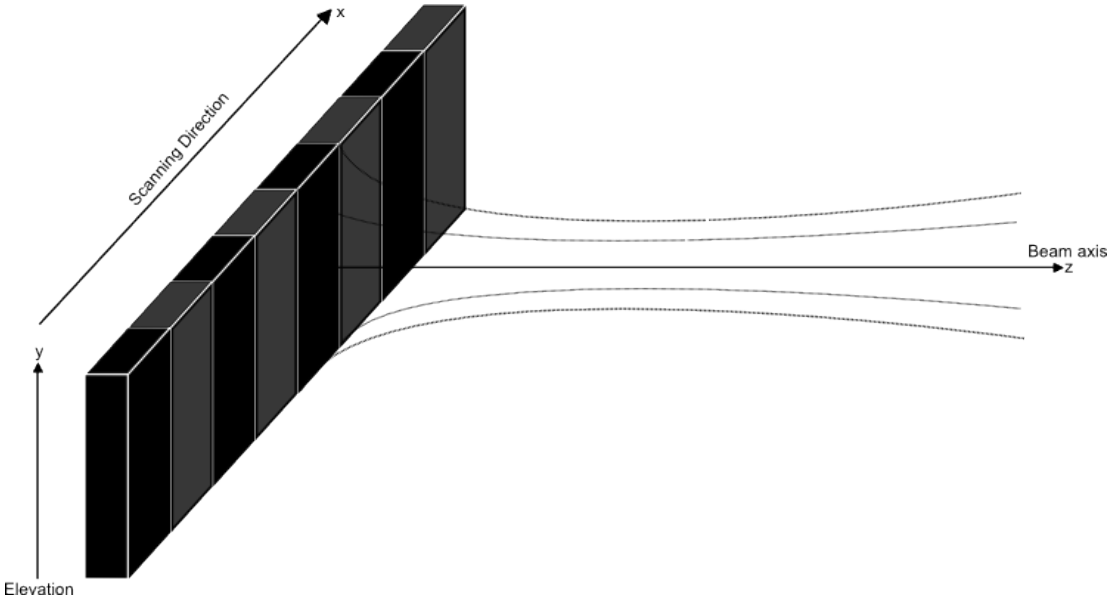

Figure 2.4: A series of elements arranged across the x-axis to form a one dimensional array.

Another advantage CMUTs have is the ease with which CMUTs can be integrated into electronic circuitry of the imaging system as compared to piezoelectric transducers, particularly when size and electrical optimization is critical to the application (endoscope and catheter based imaging, for example). A third advantage is the high depth resolution CMUTs have due to their broader bandwidth. [15]

Arrays are a combination of many small transducers that are excited to steer and focus an ultrasound beam at a certain point. This is achieved by controlling the signal delay and weight of each element to electronically focus beams at the desired depths.

2.3.2 One Dimensional Arrays

Figure 2.4 shows an example of a one dimensional array. It consists of a series of elements (typically between 32 to 300 elements), arranged across the x axis. In this particular example, the array is capable of electronic beam steering the the xz plane (often referred to as the azimuth). An acoustic lense helps maintain a certain focal length in the yz plane (often referred to as the elevation). The z axis is referred to as the nominal beam axis. Through beam steering as well as focusing with this one dimensional array, a two dimensional scan of the xz plane is possible.

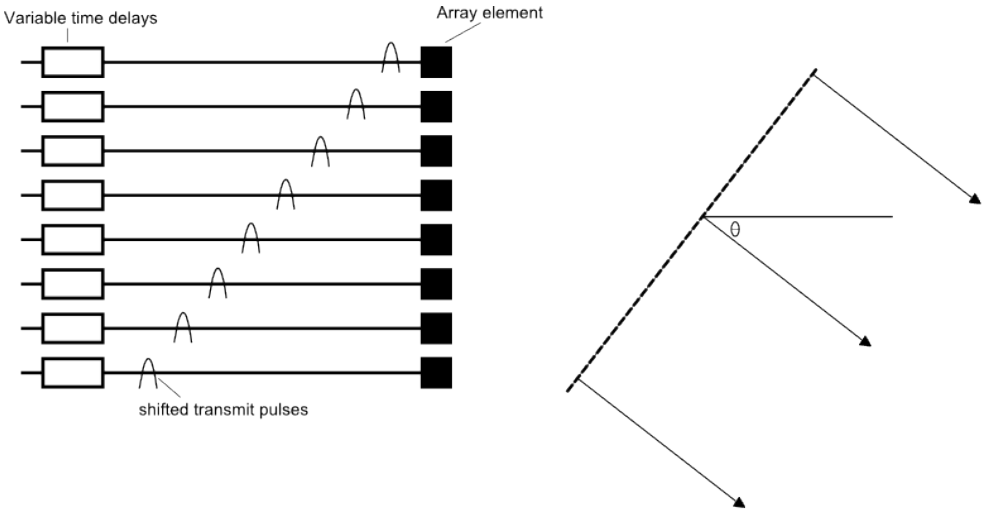

Figure 2.5: Applying time delays to achieve beam steering.[29]

Beam steering is possible by placing a linear phase across the array elements. With a linear phase at an angle θ_s from the z axis, a beam can be steered at an angle of θ_s. This is illustrated in Figure 2.5.

Beam focusing can be achieved by adding time delayed pulses in a manner simulating the effect of a lens. This is illustrated in Figure 2.6. The time delays τ_n to focus each element n are:

$$\tau_n = \frac{r - \sqrt{(x_r^2 - x_n^2 + z_r^2)}}{c} + t_0 \tag{2.24}$$

where c is the speed of sound, and r is the distance from the origin to the desired focal point:

$$r = \sqrt{x_r^2 + z_r^2} \tag{2.25}$$

x_n is the distance from the origin to the center of element n and t_0 is a constant delay added to avoid negative delays (since they are physically unrealizable).

2.3.3 Two Dimensional Arrays

While one dimensional arrays are only capable of focusing/steering in azimuth and are therefore limited to scanning in two dimensions, a two dimensional array is capable of

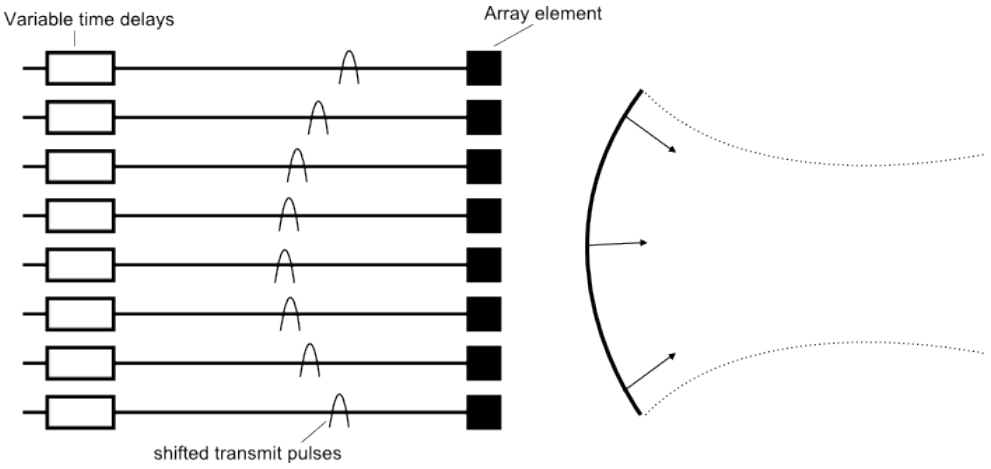

Figure 2.6: Applying time delays to achieve beam focusing. [29]

focusing and steering in three dimensions.

Figure 2.7 shows the geometry of a two dimensional array. The directions to the field point shown are u and v, and the steering directions can be written as:

$$u_s = \sin\theta_0 \cos\phi_0 \tag{2.26}$$

$$v_s = \sin\theta_s \cos\phi_s \tag{2.27}$$

where θ_0, θ_s, ϕ_0, and ϕ_s are the initial azimuthal angle, the steered azimuthal angle, the initial polar angle, and the steered polar angles respectively.

Focusing and steering is achieved in the same way it's done with one dimensional arrays: by introducing the appropriate time delay for each element. The time delay τ_{mn} needed to focus each element mn is given by:

$$\tau_{mn} = \frac{r}{c}\left[1 - \sqrt{\left[\left(\frac{u_0 - mp_x}{r}\right)^2 + \left(\frac{v_0 - np_y}{r}\right)^2 + \cos^2\theta_0\right]} - t_0\right] \tag{2.28}$$

where the focal point is defined by r as well as $\cos u_0$ and $\cos v_0$.

Fully addressed two dimensional arrays present a challenge when it comes to fabrication. While a typical one dimensional array may have 64 elements, a two dimensional array may

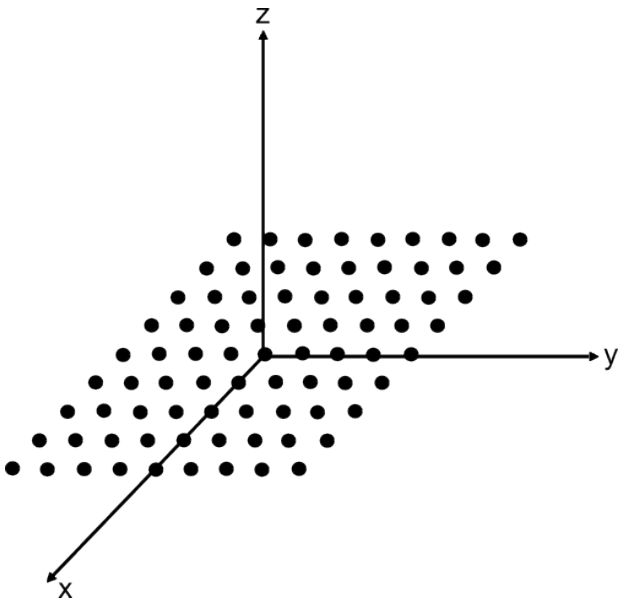

Figure 2.7: Geometry of the most basic two dimensional array. [29]

have 64^2 elements. An array with that many elements will require 4096 voltage pulsers and 4096 pre-amplifiers, which can be challenging to fit into a relatively small device.

There are many ways to simplify the design of two dimensional arrays if one is willing to compromise on image quality. By using a ring array, a sparse array, synthetic phased array, or a row-column addressing, the element design can be greatly simplified.

A ring array is a set of individually addressable elements (usually 64 or 128) arranged in a ring. Since the elements are arranged in two dimensions, a three dimensional scan is possible. The area used for transmission and reception of ultrasound waves is relatively small, and therefore this method suffers from lower signal to noise ratio (SNR).

In a sparse array, only a subset of the total elements is used to transmit and receive ultrasound waves. By reducing the number of elements, the system as a whole is simplified. The selection of the right elements to use is important as it will determine the width of the beam as well as the pitch and grating lobes. Although it usually presents with a higher SNR than a ring array, it still faces the same issue of having a relatively lower SNR due to less area beig used to transmit and receive ultrasound waves.

Synthetic phased array imaging is achieved by transmitting and receiving ultrasound from individual elements sequentially. By getting data from each element as it transmits an ultrasound signal and receives its own wave's reflection, it is possible to use this data to

reconstruct an image. The transmit power for this method is greatly reduced and therefore the SNR is reduced. Data acquisition is more time consuming in this method.

2.3.4 Row-Column Overview

This method was proposed by Morton [19], where a pair of orthogonally positioned one dimensional arrays of rows and columns (Figure 2.8) are used instead of the fully addressed two dimensional array. One set of one dimensional arrays was responsible for transmit beamforming and the other for receive beamforming. A line of focus, adjustable in both depth and azimuth, is generated in a manner similar to one dimensional transmit beamforming by the column array. Receive beamforming is achieved when the sound reflected from the object being imaged is received by the row array. Receive one dimensional array performs software beamforming so a B-mode image can be reconstructed in each transmit event, forming a complete three dimensional images after the final transmit event.

An $N \times N$ two dimensional array can be designed with only $2N$ connections when this row-column technique is used, as opposed to N^2 connections with the fully addressed one. Furthermore, according to Rasmussen [22], for any fixed number of active elements, the row-column addressing scheme produces higher quality ultrasound images as compared to the fully addressed one.

Since row-column only focuses in azimuth for transmit and elevation for receive, beamforming relies on natural focusing for elevation during transmit and azimuth during receive. Therefore, the focusing power for row-column beamforming scheme is limited. Pressure near the transducer significantly varies as sound emitted from different parts of the transducer interferes constructively and destructively. The variation in pressure decreases as sound travels away from the transducer, creating a varying beam profile that changes the response of the imaging system with depth.

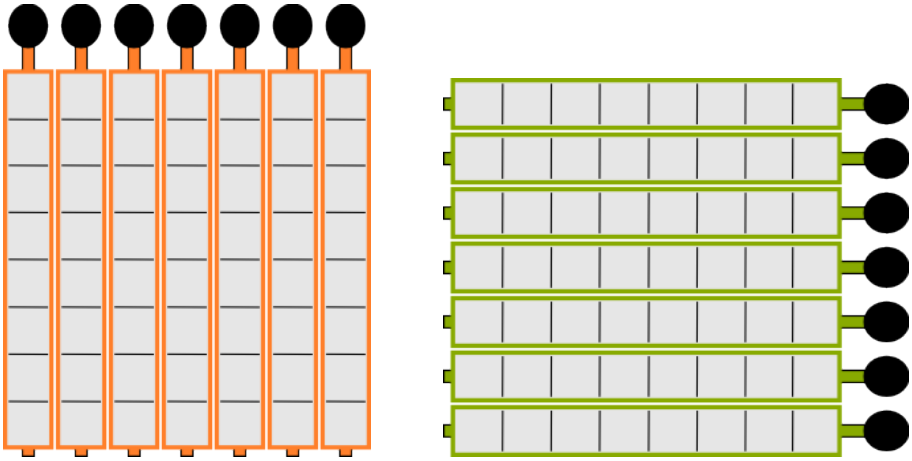

(a) 1-D columns

(b) 1-D rows

(c) Row-column arrangement

Figure 2.8: Schematic of the row-column setup. (a) shows a set of N one dimensional column arrays with N connections. (b) shows a set of N one dimensional row arrays with N connections. (c) shows the two sets of row-column arrays merged together forming a two dimensional array with $2 \times N$ connections.

Chapter 3

Joint Image Formation and Noise Modeling and Characterization

Although the row-column method was proposed more than a decade ago [19], there has been no formal attempt at working out a mathematical model for a joint image formation and noise model of row-column systems. This chapter will establish a mathematical model for characterizing the image formation and noise aspects of row-column systems. First we will provide a mathematical formulation of how an image is formed. We will then formulate a statistical model for the speckle noise component of the image formation model. We will then validate our choice by quantitatively evaluating how well our proposed statistical model fits a real data sample as opposed to other models from literature.

3.1 Image Formation

Equation 3.1 describes how a true image is observed when the row-column technique is used:

$$g(r,\theta,\phi) = M(r,\theta,\phi)[f(r,\theta,\phi) * h(r,\theta,\phi)u_m(r,\theta,\phi) + u_a(r,\theta,\phi)] \tag{3.1}$$

where r, θ, and ϕ denote the radial distance, the azimuthal angle, and the polar angle respectively. The term $g(r,\theta,\phi)$ is the observed image, $M(r,\theta,\phi)$ is the sampling function, $f(r,\theta,\phi)$ is the tissue reflectivity function, $h(r,\theta,\phi)$ is the spatially dependent point spread function (PSF); a function that describes the response of an imaging system to a point source, $u_m(r,\theta,\phi)$ is the multiplicative noise, $u_a(r,\theta,\phi)$ is the additive noise, and $*$ is the convolution operator.

To express (3.1) in the more common Cartesian form, the spherical coordinates are converted using the equations:

$$\begin{aligned} x &= r\sin(\theta)\cos(\phi) \\ y &= r\sin(\theta)\cos(\phi) \\ z &= r\cos(\theta) \end{aligned} \tag{3.2}$$

where x, y, and z are the Cartesian coordinates.

Using (3.2), (3.1) can be expressed as:

$$g(x,y,z) = M(x,y,z)[f(x,y,z) * h(x,y,z)u_m(x,y,z) + u_a(x,y,z)]. \tag{3.3}$$

The observed image g from a row-column scan is a series of fan-beams of 'readings', originating from the ultrasound source, in a three dimensional black box (the region of interest). Figure 3.1 shows a visualization of these fan-beams and how they result in image formation. The sampling function M determines how the continuous space in the region of interest is reduced to a discrete volume. The tissue reflectivity function f describes the studied object's reflection response to acoustic waves. The point spread function h is analogous to the impulse response in linear systems, it describes the response of an imaging system to a point source (this will be discussed more in Chapter 4). Multiplicative noise u_m and additive noise u_a will be discussed in the next section.

3.2 Noise in row-column Ultrasound Imaging

There are two types of noise represented in the image formation model (3.1): multiplicative and additive noise. Multiplicative noise is due to coherence interference that causes the pattern referred to as speckle noise [29]. Additive noise is mostly due to sensor noise. The effect of additive noise on the tissue reflectivity function is not as significant as multiplicative noise and is therefore often ignored [18]. This section will focus on speckle noise.

3.2.1 Speckle Noise

Scans from all coherent imaging modalities present with speckle noise. This noise is a byproduct of the interfering echoes of a transmitted waveform reflected from the studied

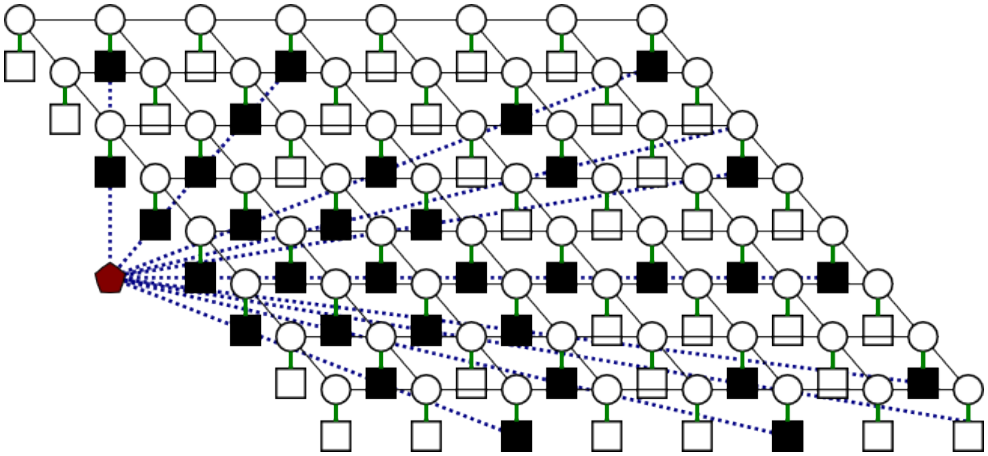

Figure 3.1: Visualizations of fan-beams. The circles represent the real image. The black squares represent the observed image. The white squares represent the observations outside the fan-beam that are not taken into consideration.

object's heterogeneities. This intricate pattern usually results from the superposition of ultrasound echoes coming with random phases and amplitudes, and scales from zero to a maximum whether the interference is constructive or destructive. [18]

There is little relationship between between speckle and macroscopic properties of the studied object, which is a distraction when ultrasound is used as a diagnostic tool. Although the random process of speckle is undesirable most of the time, it can still give useful information. In medical diagnostics for example, the statistics of speckle can provide information on tissue composition or type since these statistics generally depend on the microstructure of tissue paranchyma [29]. However, the fact that speckle tends to reduce image contrast and obscure some image details which in turn effects the readability of ultrasound images are major reasons why speckle noise is unwanted.

Research into the use of statistical analysis of speckle as a tool for speckle removal was given a great push by Goodman's paper [31], where statistical mechanism of laser speckle formation was first presented. This study was then revised by other researchers to specifically account for speckle in ultrasound [18]. These studies recommended the use of linear filters to reduce speckle noise.

Many more filtering techniques were proposed, each improves upon the drawbacks of the previous one but still comes at a cost. Jane proposed an algorithm where they applied logarithmic transformation to convert the multiplicative nature of speckle into additive noise, applying Wiener filter on the transformed image and ending with an exponential

transformation [8]. This algorithm had the advantage of being extensive in the sense that any filter besides Wiener filter can be used.

The discovery of the Wavelet transform gave rise to a wide variety of tools for image despeckling [18]. In particular, techniques that adopted Jane's algorithm structure of replacing the Wiener filter with wavelet denoising, have shown considerable success [18]. These are referred to as homomorphic wavelet despeckling (HWDS) methods.

Michailovich's study, however, showed that proper statistical analysis of speckle noise provides the best basis for ultrasound image despeckling techniques [18]. They have shown that the general assumption, ubiquitous in all these techniques, that consider the log transformed noise to be white-Gaussian noise tends to oversimplify the despeckling framework and leads to inadequate performance of these methods.

According to the study done by [18], there are three main cases that can help determine which statistical model is a better fit for speckle noise. If a background of relatively weak scatterers has a structure of specular reflectors superimposed on it, the noise will most likely follow Rician distribution. If there is a large number of independent scatterers, then noise will most likely follow the Rayleigh distribution. If the number of scatterers is low or the spatial locations of scatterers are not independant, which is often the case, then the noise distribution will likely deviate from the Rayleigh distribution.

A number of distributions were proposed for the third case - when the number of scatterers is low or the spatial locations of scatterers are not independent - including the Nakagami distribution, the Weibull distribution, and the generalized gamma distribution. We will investigate the best fit distribution using data generated from a row-columnn ultrasound system designed and built by the Advanced Micro-/Nano- Devices Lab at the University of Waterloo.

3.2.2 Generalized Noise Model

To better understand speckle noise, we will derive a generalized model for it and try to find a statistical description for said model. First, we will simplify the image formation model from (3.3) to:

$$g(x, y, z) = f(x, y, z)u_m(x, y, z) + u_a(x, y, z) \tag{3.4}$$

where $g(x, y, z)$ is the noisy observation, $f(x, y, z)$ is the noise-free image, $u_m(x, y, z)$ is the multiplicative noise due to coherent interference, and $u_a(x, y, z)$ is the additive noise (sensor noise, etc.).

The effects of additive noise are considerably smaller than multiplicative noise [18]. Therefore, the additive noise term can be removed from (3.4) and $g(x, y, z)$ can be expressed as:

$$g(x, y, z) = f(x, y, z)u_m(x, y, z). \tag{3.5}$$

Taking the log of (3.5) would turn the multiplication into a simple addition problem:

$$\log\left(g(x, y, z)\right) = \log\left(f(x, y, z)\right) + \log\left(u_m(x, y, z)\right). \tag{3.6}$$

3.2.3 Statistical Modeling and Characterization of Noise in row-column Measurements

As previously mentioned, the mechanisms of the speckle formation in laser imaging [31] and ultrasound imaging are similar, and the tissue composition and type of the studied object generally define the statistical description of speckle [18]. We will test a number of statistical distributions proposed in the literature on a set of raw data acquired using the row-column system designed and built by the Advanced Micro-/Nano- Devices Lab.

The data was acquired by a customized imaging system built using the PCI eXtensions for Instrumentation (PXI) platform. A row-column addressing capacitive micromachined ultrasonic transducers array (RC-CMUTs) was used. The 32 by 32 two dimensional array has a center frequency of 5.9MHz, an aperture size of 4.8mm by 4.8 mm with a 150μm pitch. The phantom imaged was a set of four wires 644 μm in diameter arranged in a way to allow for a scan of their cross sections.

Five different regions of the captured measurements (shown in Figure 3.2) were used to find the best distribution that fits row-column measurements. Model fitting was done through MATLAB, and the log likelihood function was used as a quantitative metric to evaluate the best fit. Figures 3.3 through 3.7 show the results of fitting Nakagami, Rayleigh, Weibull, generalized gamma, and exponential distributions into the five different regions. Table 3.1 summarizes the log likelihood of each fit.

Visual analysis of the model fitting shows that Nakagami and generalized gamma provide the closest fit to all five regions, and exponential giving the worst fit. This is also supported by quantitative analysis, with Nakagami and generalized gamma having the highest log likelihood and exponential having the lowest. However, in four out of five regions, the generalized gamma distribution had a higher log likelihood, and so we will build our noise statistical model based on the assumption that noise follows the generalized gamma distribution.

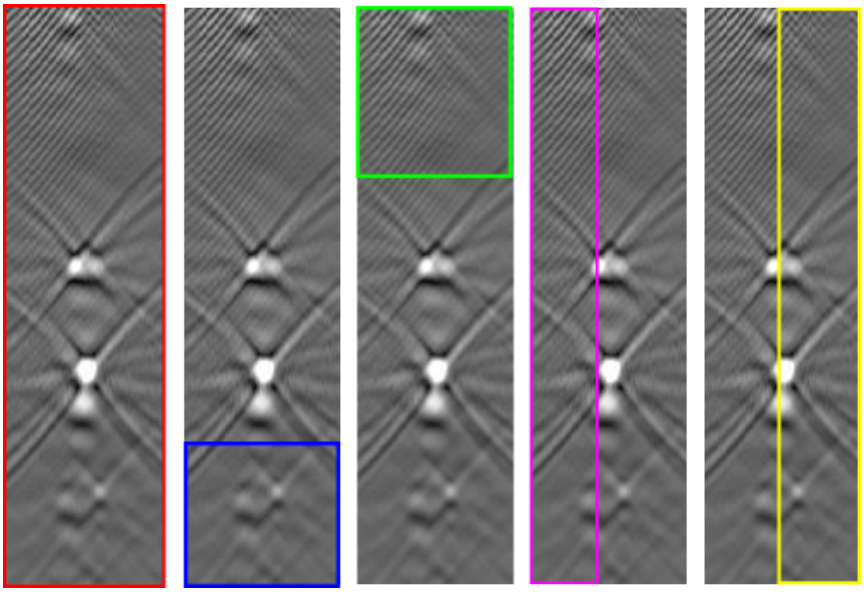

Figure 3.2: Chosen regions from the row-column measurements that were used to perform statistical modeling.

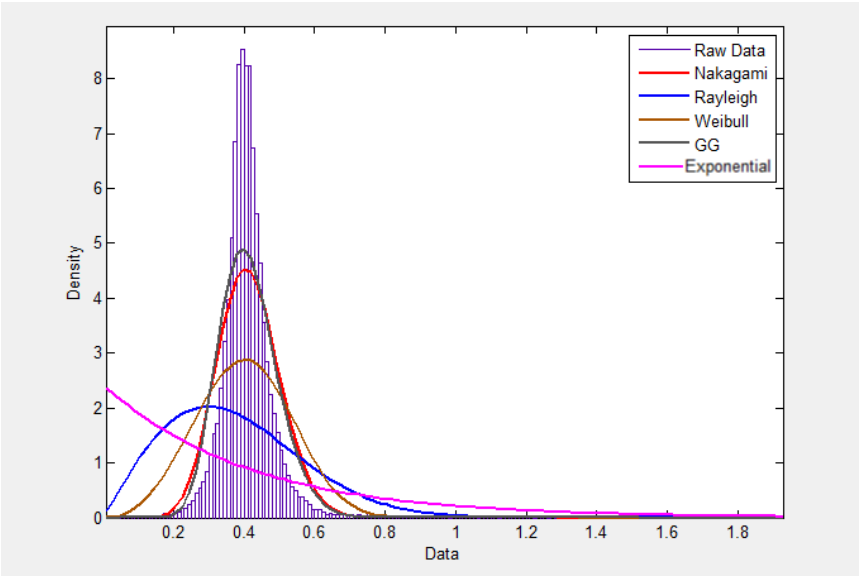

Figure 3.3: A fit of Nakagami, Rayleigh, Weibull, generalized gamma, and exponential distributions on the first region.

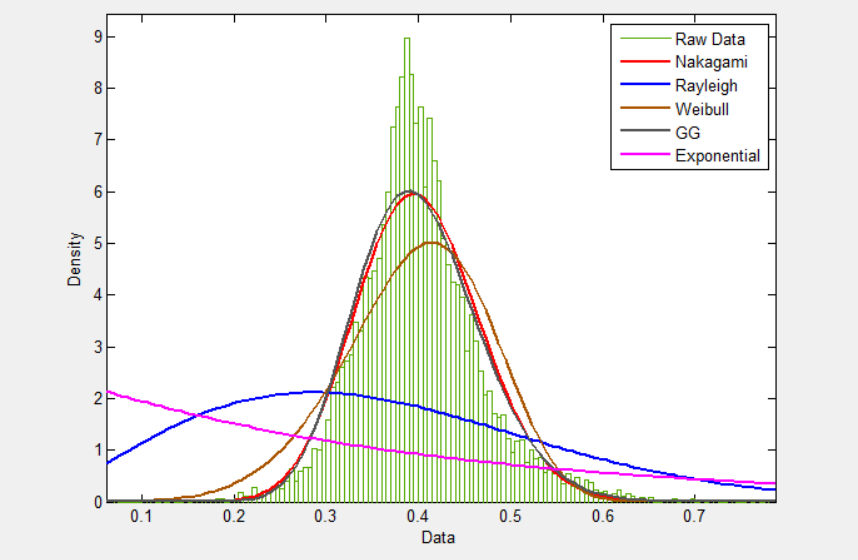

Figure 3.4: A fit of Nakagami, Rayleigh, Weibull, generalized gamma, and exponential distributions on the second region.

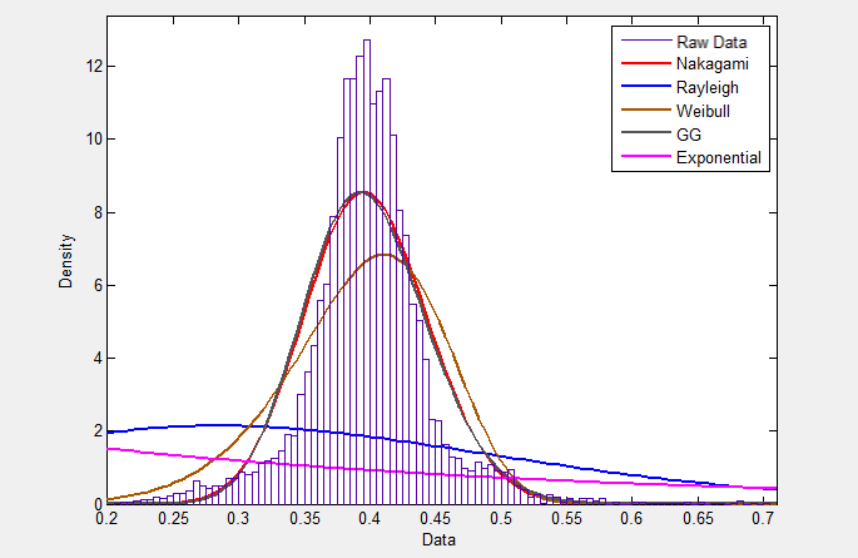

Figure 3.5: A fit of Nakagami, Rayleigh, Weibull, generalized gamma, and exponential distributions on the third region.

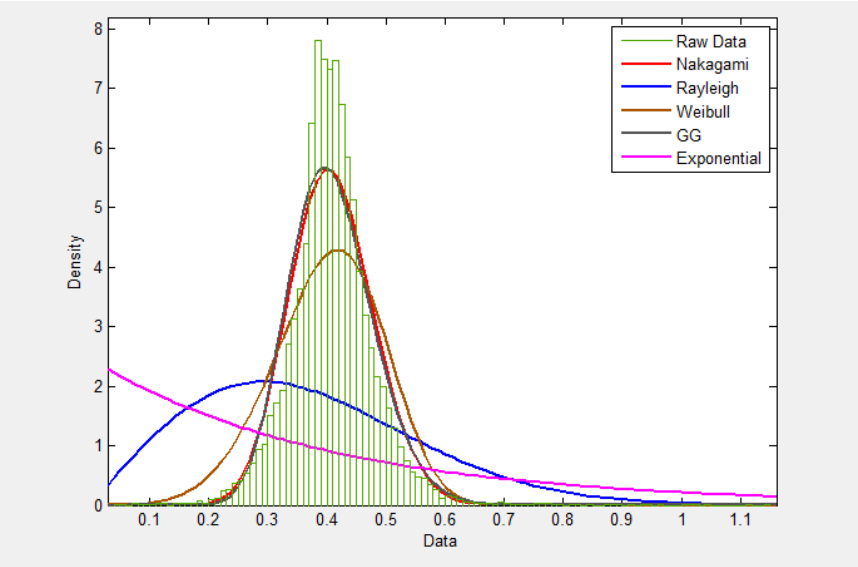

Figure 3.6: A fit of Nakagami, Rayleigh, Weibull, generalized gamma, and exponential distributions on the fourth region.

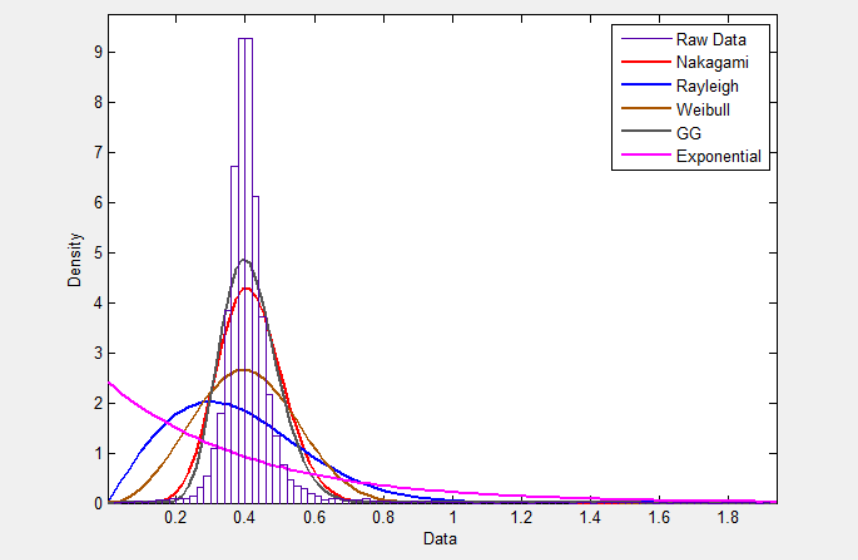

Figure 3.7: A fit of Nakagami, Rayleigh, Weibull, generalized gamma, and exponential distributions on the fifth region.

Table 3.1: Log likelihood of different distributions fit to the five chosen regions. Higher values of log likelihood indicate better fit.

Distribution	Region 1	Region 2	Region 3	Region 4	Region 5
Nakagami	31074	11732	**12903**	16547	14873
Rayleigh	15530	5153	4646	7292	7672
Weibull	23460	10942	11979	14768	10742
Generalized gamma	**33164**	**11747**	12878	**16556**	**16633**
Exponential	-3449	-773	-617	-1395	-1776

The pdf of the generalized gamma distribution is given by:

$$p_z(z) = \frac{\gamma z^{(\gamma v-1)}}{\alpha^{\gamma v}\Gamma(v)} \exp\left(-(\frac{z}{\alpha})^{\gamma} \right), \qquad z \geq 0, \alpha, v, \gamma > 0 \tag{3.7}$$

where $\Gamma(\cdot)$ is the gamma function, an extension of the factorial function with the argument shifted by one. For integers, the gamma function is given by:

$$\Gamma(n) = (n-1)! \tag{3.8}$$

and for all complex numbers with positive real parts, it is define as:

$$\Gamma(v) = \int_0^{\infty} x^{v-1} \exp(-x) \mathrm{d}x \tag{3.9}$$

This distribution is very appealing as it contains several distributions as special cases, this is summarized in Table 3.2. Following the Generalized Gaussian assumption, the noise samples of the logarithmic transformed speckle in Equation 3.6 is given by the pdf:

$$p(y) = \frac{\gamma}{\Gamma(v)} \exp\left[\gamma v(y - \ln\sigma) - \exp\left[\gamma(y - \ln\sigma)\right] \right] \tag{3.10}$$

To put this in context of the three dimensional row-column imaging system, we propose the following noise model to characterize the log-transformed speckle noise:

$$p_{RC}(I(x,y,z)) = 2\exp\left[(2I(x,y,z) - \ln 2\sigma^2) - \exp\left[2I(x,y,z) - \ln 2\sigma^2\right] \right] \tag{3.11}$$

where $I(x,y,z)$ denotes voxel intensity at point (x,y,z), and σ is the standard deviation of voxel intensities.

Table 3.2: List of distributions that are special cases of the generalized gamma distribution

γ value	v value	Distribution
2	1	Rayleigh
1	1	Exponential
2	v	Nakagami
γ	1	Weibull
γ	$v \to \infty$	log-Normal

3.3 Summary

In this chapter, we developed a mathematical model for a joint image formation and speckle noise in row-column systems. We proposed an expression for how an image is observed in a row-column system, taking into account the system's point spread function as well as speckle noise. We then gave a brief overview of speckle in literature with a focus on the importance of proper statistical modeling of speckle to speckle removal. After that we used the proposed image formation expression to come up with a generalized noise model, and using real ultrasound data from a row-column based system we defined a statistical model for both speckle noise and the log transformed speckle noise. Now that we have a mathematical model for a joint image formation and speckle noise for ultrasound imaging systems based off of the row-column method, we will now find a mathematical derivation of the beam profile for these systems.

Chapter 4

Beam Profile Modeling and Characterization

Given the image formation model for row-column imaging systems presented in Equation 3.1, and the noise model and characterization arrived at in Equation 3.11, the last component that remains to be modeled and characterized is the point spread function h. The point spread function of a row-column ultrasound imaging system h describes the system's beam profile and has a tremendous impact on the performance of the system; hence, it is important to have a better understanding and quantitative characterization of the point spread function. The goal of this chapter is to provide a mathematical derivation for modeling and characterizing a row-column system's beam profile, as well as study a row-column system's beam profile characteristics at different imaging depths through simulation.

4.1 Linear Systems Theory and Acoustic Systems

A common practice in electrical engineering is to fully characterize a linear electrical system by its impulse response. Applying a delta function as an input to a system will result in the system's impulse response $h(t)$ as output. Given this characteristic impulse response, estimating a system's output $y(t)$ with input $x(t)$ using basic linear systems theory is possible [9]. The relationship between the input $x(t)$, output $y(t)$, and impulse response $h(t)$ is given by:

$$y(t) = h(t) * x(t) = \int_{-\infty}^{\infty} h(\theta)x(t-\theta)\mathrm{d}\theta \tag{4.1}$$

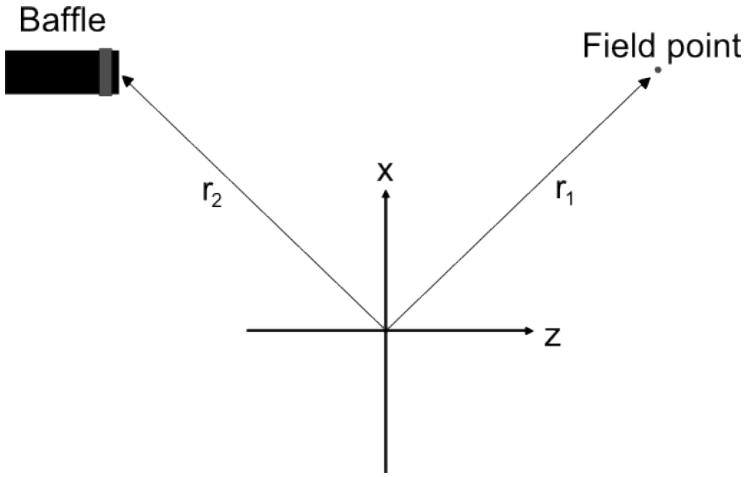

Figure 4.1: Basic setup of an ultrasound system [14].

where $*$ denotes time convolution.

Linear acoustic systems can be characterized in a similar manner [14], where the impulse response is referred to as the point spread function. For ultrasound imaging systems, this point spread function characterizes the system's beam profile. Given the basic setup for an ultrasound system 4.1, the position of the baffle will be denoted by $\vec{r}_2$, the position of the hydrophone that will measure the acoustic output of the transducer (the 'field point') will be denoted by $\vec{r}_1$, a medium with density ρ_0, and a constant speed of sound c.

Using Huygens' principle [9], where every point on the radiating surface is the origin of an outgoing spherical wave, we can get a perception of the sound field at a fixed time instance. Each of the spherical waves are given by:

$$SP(\vec{r}_1) = \delta\big(t - \frac{|\vec{r}_2 - \vec{r}_1|}{c}\big) \tag{4.2}$$

where t is the time for the snapshot of the spatial distribution of the pressure.

By observing the pressure waves at a fixed point in space over time and summing all waves that pass through that point, the beam profile of a linear acoustic system can be found.

A formal derivation of the beam profile will be formulated in the next section.

4.2 Mathematical Derivation

Building on the Huygens' principle assumption and equation 4.2 from the previous section, the pressure field generated by an aperture with geometry S can be expressed as:

$$p(\vec{r}_1, t) = \frac{\rho_0}{2\pi} \int_S \frac{\frac{\partial v_n(\vec{r}_2, t - \frac{|\vec{r}_1 - \vec{r}_2|}{c})}{\partial t}}{|\vec{r}_1 - \vec{r}_2|} \mathrm{d}S \tag{4.3}$$

where v_n is the velocity normal to the transducer surface [9].

The derivation in (4.3) assumes linearity and propagation in a homogeneous medium. The radiating aperture is also assumed to be flat, meaning no re-radiation from scattering and reflection takes place [14].

Exchanging the integration and partial derivative, equation 4.3 can be rewritten as:

$$p(\vec{r}_1, t) = \frac{\rho_0}{2\pi} \frac{\partial \int_S \frac{v_n(\vec{r}_2, t - \frac{|\vec{r}_1 - \vec{r}_2|}{c})}{|\vec{r}_1 - \vec{r}_2|}}{\partial t} \mathrm{d}S. \tag{4.4}$$

Given the relationship between pressure and velocity potential from Chapter 2, the velocity potential can be expressed as:

$$\Psi(\vec{r}_1, t) = \int_S \frac{v_n(\vec{r}_2, t - \frac{|\vec{r}_1 - \vec{r}_2|}{c})}{2\pi |\vec{r}_1 - \vec{r}_2|} \mathrm{d}S \tag{4.5}$$

We can then separate the excitation pulse from the transducer geometry by introducing a time convolution with a delta function:

$$\Psi(\vec{r}_1, t) = \int_S \int_T \frac{v_n(\vec{r}_2, t_2) \delta(t - t_2 - \frac{|\vec{r}_1 - \vec{r}_2|}{c})}{2\pi |\vec{r}_1 - \vec{r}_2|} \mathrm{d}t_2 \mathrm{d}S \tag{4.6}$$

where δ is the Dirac delta function.

If we assume that the surface velocity is uniform (i.e. it is independent of $\vec{r}_2$) over the aperture [14], then (4.6) becomes:

$$\Psi(\vec{r}_1, t) = v_n(t) * \int_S \frac{\delta(t - \frac{|\vec{r}_1 - \vec{r}_2|}{c})}{2\pi |\vec{r}_1 - \vec{r}_2|} \mathrm{d}S \tag{4.7}$$

where * denotes deconvolution.

The integral in equation 4.7 is the point spread function from equation 3.1:

$$h(\vec{r}_1, t) = \int_S \frac{\delta(t - \frac{|\vec{r}_1 - \vec{r}_2|}{c})}{2\pi|\vec{r}_1 - \vec{r}_2|} \mathrm{d}S \tag{4.8}$$

and characterizes the three dimensional beam profile of an ultrasound system for a particular transducer geometry S.

From equation 4.8, the beam profile is spatially dependant, which is consistent with the varying pressure field emanating from a transducer according to equation 4.3. Pressure near the transducer significantly varies as sound emitted from different parts of the transducer interferes constructively and destructively, and this variation decreases as sound travels across the medium. Therefore, to have a beam profile that varies with depth makes sense.

4.3 Simulation

Deriving a full mathematical expression for the beam profile of a row-column system is incredibly complex, and as seen in (4.8), beam profile is directly dependant on the transducer geometry. However, it is possible to simulate a row-column system's beam profile using computer modeling.

To numerically model and characterize the beam profile characteristics of the row-column system, the Field II simulation toolkit [10] was used here as it is a widely used toolkit in research literature for simulating ultrasound system characteristics. For illustrative purposes, it is used here to characterize and estimate the beam profiles of the row-column system with a 5mm x 5mm, 32x32 element row-column array at three different depths away from the transducer: 5mm, 10mm, and 20mm.

To estimate the beam profile of a row-column system at a particular point in space, the transducer aperture and geometry are first defined. Apertures for emission and reception were set, and a point phantom at the required depth (analogous to field point denoted by $\vec{r}_1$ earlier) is created. A linear sweep is then made, followed by the generation of a point scatterer. The beam profile is then found using the same mathematical basis presented in equation 4.8.

4.4 Results

Figures 4.2 and 4.3 show the output of the Field II testing done in MATLAB, where the simulation of the beam profile of a 5mm×5mm, 32×32 element row-column array at three different depths away from the transducer: 5mm, 10mm, and 20mm.

Looking at Figure 4.2, we can see that the profile spike gets wider as we move away from the transducer. This is consistent with the discussion at the end of Section 4.2: the pressure waves weaken as sound travels away from the transducer and the ability to focus becomes more difficult.

Figure 4.3 shows the reduction of beam focus in more detail. The -6dB resolution weakens in spot size from 0.5mm to 0.9mm as we move from 5mm to 20mm away from the transducer. The effects of interference of pressure waves decrease as it weakens the farther you are from the transducer, and so focusing becomes more challenging. Looking at the profiles in Figure 4.3 also reveals the set of side lobes below -30dB getting larger is we move away from the transducer, an indicator of the reduction of natural focus with depth.

The side lobes shape shown in Figure 4.2 is consistent with the beam profile of a typical row-column array [29], since this shape is highly influenced by the natural focusing tendency of the row-column's beamforming method [9].

4.5 Summary

In this chapter, we used Huygens' principle assumption and linear systems theory to derive a mathematical expression for the row-column system's spatially varying point spread function which describes the system's beam profile. We used Field II MATLAB toolkit to perform some beam profile simulations to see if our formulation is consistent with literature on beam profiles. With the formulations from chapter 3, we now have a complete characterization model. The next chapter will conclude this thesis.

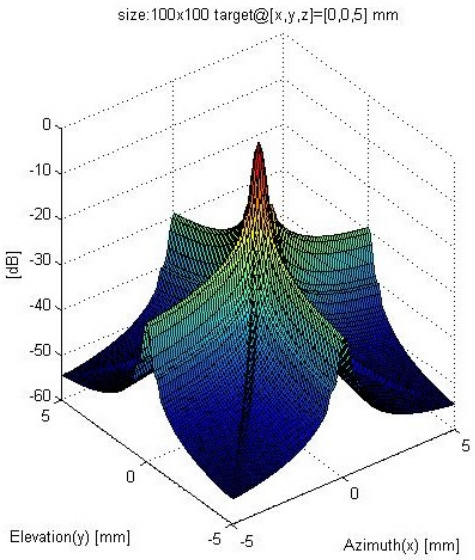

(a) Beam profile at 5mm

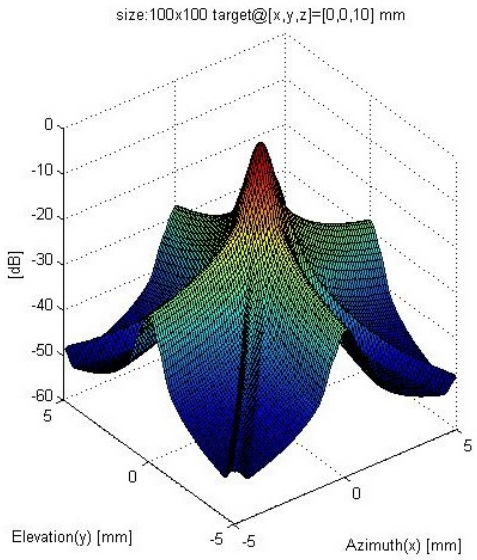

(b) Beam profile at 10mm

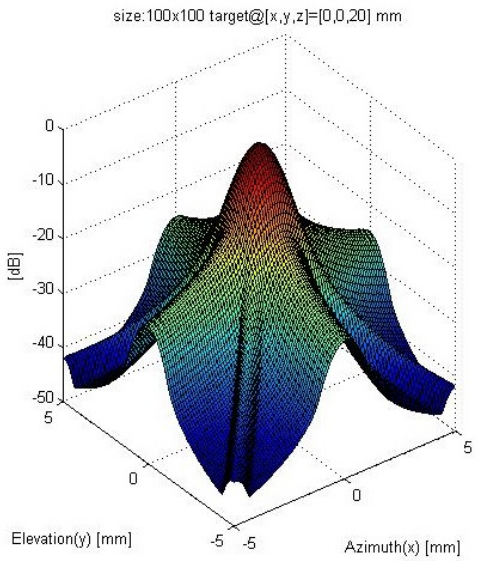

(c) Beam profile at 20mm

Figure 4.2: Results of Field II MATLAB simulations. Beam profiles of a row-column system at different depths away from the tranducer. The profile spike gets more wide as its pressure decreases away from the transducer.

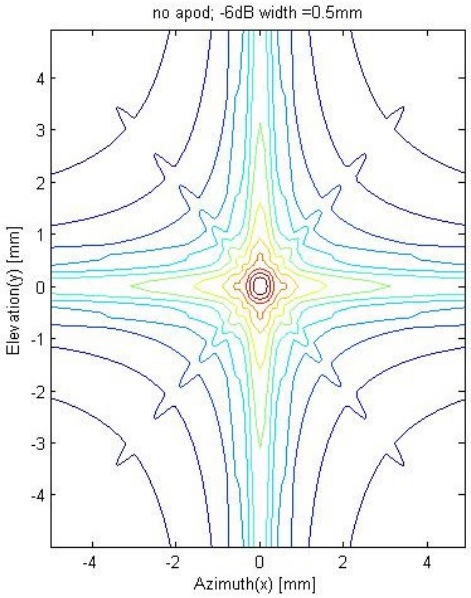

(a) Beam profile at 5mm

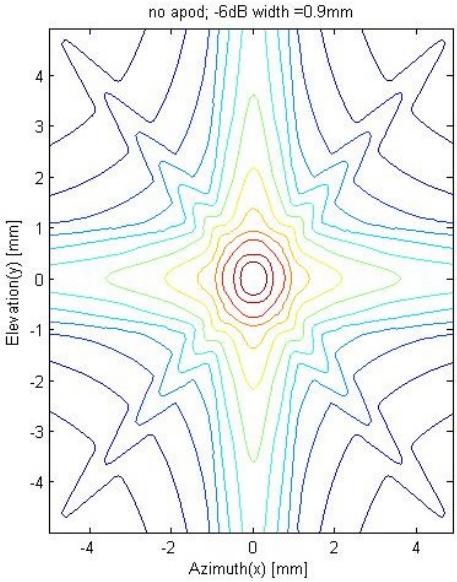

(b) Beam profile at 10mm

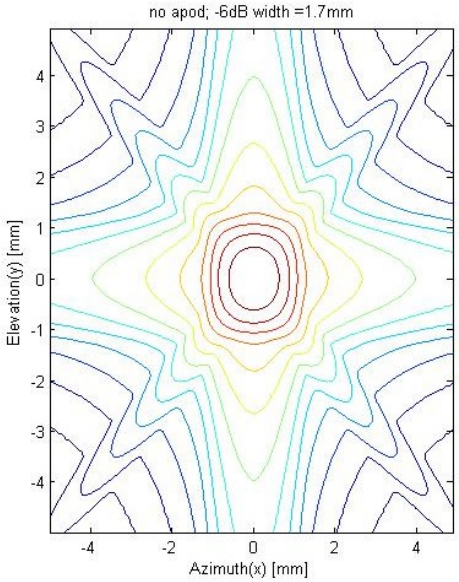

(c) Beam profile at 20mm

Figure 4.3: Results of Field II MATLAB simulations. Beam profiles of a row-column system at different depths away from the tranducer. The characteristic sidelobes are consistent with row-column beamforms.

Chapter 5

Conclusion and Future Work

5.1 Summary

In this thesis, we proposed a characterization framework for ultrasound imaging systems that are based on the row-column method.

In Chapter 3, we developed a mathematical model for a joint image formation and speckle noise in row-column systems. We proposed an expression for how an image is observed in a row-column system, taking into account the system's point spread function as well as speckle noise. We then gave a brief overview of speckle in literature with a focus on the importance of proper statistical modeling of speckle to speckle removal. After that we used the proposed image formation expression to derive a generalized noise model, and using real ultrasound data from a row-column based system we defined a statistical model for both speckle noise and the log transformed speckle noise.

In chapter 4, we mathematically derived a characterization of a row-column system's beam profile. First we briefly introduced acoustic systems in context with linear system theory. Then, using Huygens' principle assumption, we arrived at a mathematical expression that characterizes the three dimensional beam profile of row-column systems. We performed simulations using the toolkit Field II to estimate the beam profile of a row-column system at different depths and discussed the results.

5.2 Future Work

The characterization model developed in this research for row-column based ultrasound systems has many potential applications that can be pursued in the future:

- **Build a more adequate image reconstruction model from data acquired with row-column based ultrasound imaging systems.** Having a mathematical representation of image formation, proper statistical model of ultrasound speckle noise, and mathematical representation of the system's beam profile would give us ample information to better compensate for the effects of the systems intrinsic imperfections.
- **Create a better metric for the comparison of different row-column based ultrasound imaging systems.** Having a mathematical representation of image formation as well as a mathematical representation of the system's beam profile would give us a more convincing metric for comparing the performance of different systems.
- **Allow for better optimization of the performance of row-column based ultrasound imaging systems.** Having a mathematical representation of image formation, proper statistical model of ultrasound speckle noise, and mathematical representation of the system's beam profile would give use enough information about a system's performance and make it easier to then optimize it.
- **Give us a better understanding of images acquired from row-column based ultrasound imaging systems.** Having a mathematical representation of image formation, proper statistical model of ultrasound speckle noise, and mathematical representation of the system's beam profile would give us a better understanding of the acquired images.

References

[1] A Achim, A Bezerianos, and P. Tsakalides. Novel bayesian multiscale method for speckle removal in medical ultrasound images. *IEEE Transactions on Medical Imaging*, 20(8):772–783, Aug 2001.

[2] Andrew Black, Pushmeet Kohli, and Carsten Rother. *Markov random fields for vision and image processing*. The MIT Press, 2011.

[3] Ameneh Boroomand, Alexander Wong, Edward Li, Daniel S. Cho, Betty Ni, and Kostandinka Bizheva. Multi-penalty conditional random field approach to super-resolved reconstruction of optical coherence tomography images. *Biomed Optics Express*, 4(10), 2013.

[4] A. IH. Chen, L.L. Wong, A. S. Logan, and J. T W Yeow. A CMUT-based real-time volumetric ultrasound imaging system with row-column addressing. *IEEE International Ultrasonics Symposium*, pages 1755–1758, Oct 2011.

[5] C. E M Demore, A Joyce, K. Wall, and G.R. Lockwood. Real-time volume imaging using a crossed electrode array. *IEEE Transactions on Ultrasonics, Ferroelectrics, and Frequency Control*, 56(6):1252–1261, June 2009.

[6] Sudipto Dolui. *Variable Splitting as a Key to Efficient Image Reconstruction*. PhD thesis, University of Waterloo.

[7] C. Fritsch, M. Parrilla, A Ibanez, R.C. Giacchetta, and O. Martinez. The progressive focusing correction technique for ultrasound beamforming. *IEEE Transactions on Ultrasonics, Ferroelectrics, and Frequency Control*, 53(10):1820–1831, October 2006.

[8] A. K. Jain. *Fundamentals of Digital Image Processing*. Prentice-Hall, Inc., Upper Saddle River, NJ, USA, 1989.

[9] Jorgen A. Jensen. *Linear descriptions of ultrasound imaging systems*.

[10] Jorgen A. Jensen. Field: A program for simulating ultrasound systems. *10th Nordic-Baltic Conference on Biomedical Imaging Published in Medical Biological Engineering Computing*, 34:351–353, 1996.

[11] Farnoud Kazemzadeh, Mohammad J. Shafiee, Alexander Wong, and David A. Clausi. Reconstruction of compressive multispectral sensing data using a multilayered conditional random field approach. *SPIE Proceedings*, 9217, 2014.

[12] A. Koch, S. Gruber, T. Scharrer, K.T. Fendt, R. Lerch, and H. Ermert. 2d transmission imaging with a crossed-array configuration for defect detection. *2012 IEEE International Ultrasonics Symposium*, pages 36–39, Oct 2012.

[13] John D. Lafferty, Andrew McCallum, and Fernando C. N. Pereira. Conditional random fields: Probabilistic models for segmenting and labeling sequence data. *Proceedings of the Eighteenth International Conference on Machine Learning*, pages 282–289, 2001.

[14] A. S. Logan, L. L. Wong, and J. T W Yeow. 2-d CMUT wafer bonded imaging arrays with a row-column addressing scheme. *IEEE International Ultrasonics Symposium*, pages 984–987, Sept 2009.

[15] Andrew Stephen Logan. *The Design, Fabrication and Characterization of Capacitive Micromachined Ultrasonic Transducers for Imaging Applications*. PhD thesis, University of Waterloo.

[16] AS. Logan, L.L.P. Wong, AIH. Chen, and J.T.W. Yeow. A 32 x 32 element row-column addressed capacitive micromachined ultrasonic transducer. *IEEE Transactions on Ultrasonics, Ferroelectrics, and Frequency Control*, 58(6):1266–1271, June 2011.

[17] O Michailovich and A Tannenbaum. Despeckling of medical ultrasound images. *IEEE Transactions on Ultrasonics, Ferroelectrics, and Frequency Control*, 53(1):64–78, Jan 2006.

[18] O Michailovich and A Tannenbaum. Blind deconvolution of medical ultrasound images: A parametric inverse filtering approach. *IEEE Transactions on Image Processing*, 16(12):3005–3019, Dec 2007.

[19] C.E. Morton and G.R. Lockwood. Theoretical assessment of a crossed electrode 2-d array for 3-d imaging. *IEEE Symposium on Ultrasonics*, 1:968–971, Oct 2003.

[20] C.S. Nageswari and K.H. Prabha. Despeckle process in ultrasound fetal image using hybrid spatial filters. *International Conference on Green Computing, Communication and Conservation of Energy*, pages 174–179, Dec 2013.

[21] A. Osman, U. Hassler, V. Kaftandjian, and J. Hornegger. An automated data processing method dedicated to 3d ultrasonic non destructive testing of composite pieces. *IOP Conference Series: Materials Science and Engineering*, 42, 2012.

[22] M.F. Rasmussen and J.A Jensen. 3-d ultrasound imaging performance of a row-column addressed 2-d array transducer: A measurement study. *IEEE International Ultrasonics Symposium*, pages 1460–1463, July 2013.

[23] J. Sanches, J.M. Bioucas-Dias, and J.S. Marques. Minimum total variation in 3d ultrasound reconstruction. *IEEE International Conference on Image Processing*, 3:597–600, Sept 2005.

[24] M. J. Shafie, A. Wong, P. Siva, and P. Fieguth. Efficient baysian inference using fully connected conditional random fields with stochastic cliques. *IEEE International Conference on Image Processing*, 2014.

[25] G Shruthi, B S Usha, and S Sandya. Article: A novel approach for speckle reduction and enhancement of ultrasound images. *International Journal of Computer Applications*, 45(20):14–20, May 2012.

[26] R. Sivakumar, M. K. Gayathri, and D. Nedumaran. Speckle filtering of ultrasound b-scan images - a comparative study between spatial and diffusion filters. *IEEE Conference on Open Systems*, pages 80–85, Dec 2010.

[27] Robert A. Smith and Luke J. Nelson. 2d transmission imaging with a crossed-array configuration for defect detection. *Insight Journal of The British Institute of NDT*, 51:82 – 87, 2009.

[28] Rajeev Srivastava, JRP Gupta, and Harish Parthasarthy. Comparison of pde based and other techniques for speckle reduction from digitally reconstructed holographic images. *Optics and Lasers in Engineering*, 48(5):626 – 635, 2010.

[29] Thomas L. Szabo. *Diagnostic ultrasound imaging: inside out.* Elsevier Academic Press, 200 Wheeler Road, 6th Floor, Burlington, MA 01803, USA, 2004.

[30] Kazuyuki Tanaka, Shun Kataoka, and Muneki Yasuda. Statistical performance analysis by loopy belief propagation in bayesian image modeling. *Journal of Physics: Conference Series*, 233(1), 2010.

[31] M. Tur, K. C. Chin, and J. W. Goodman. When is speckle noise multiplicative? *Appl. Opt.*, 21(7):1157–1159, Apr 1982.

[32] Shibin Wu, Qingsong Zhu, and Yaoqin Xie. Evaluation of various speckle reduction filters on medical ultrasound images. *Engineering in Medicine and Biology Society*, pages 1148–1151, July 2013.

[33] Futian Yao, Yuntao Qian, Zhenfang Hu, and Jiming Li. A novel hyperspectral remote sensing images classification using gaussian processes with conditional random fields. *International Conference on Intelligent Systems and Knowledge Engineering*, pages 197–202, 2010.